

# PZT AND PNZT-BASED THIN FILM CAPACITORS AND TRANSMISSION LINES FOR MICROWAVE INTEGRATED CIRCUIT APPLICATIONS

Z. Awang and S. Sulaiman

Microwave Technology Centre, University Technology MARA, 40450 Shah Alam, Malaysia  
zaiki.awang@gmail.com, anisafiq2@yahoo.com

**Keywords:** Thin film capacitor, co-planar waveguide transmission line, PZT, PNZT, thin dielectric films, monolithic microwave integrated circuits.

**Abstract:** Ferroelectric materials have superior dielectric properties but the processing conditions of thin ferroelectric films influence their dielectric properties and thus affect the performance of devices which employ them. A detailed characterization is carried out for lead zirconate titanate (PZT) and lead niobate zirconate titanate (PNZT) thin films in this work by employing planar-circuit structures. The films were applied to built microwave capacitors and co-planar waveguide transmission lines. S-parameter measurements were performed from 40 MHz to 20 GHz using wafer probes in conjunction with a vector network analyzer. The results show the loss tangent and relative permittivity of the films vary with frequency, with typical permittivity values of the order of 110 to 350 and 200 to 780 for PZT and PNZT, respectively, over the said frequency range. The investigation revealed the effect of dielectric polarization of the films over the broad frequency range. The transmission lines showed acceptable insertion losses of the order of 17 dB from 5 to 20 GHz for lines of length 100  $\mu\text{m}$  and width 5  $\mu\text{m}$  fabricated on PNZT films 1  $\mu\text{m}$  thick. These figures demonstrate the feasibility of using thin ferroelectric films as a new substrate material for monolithic microwave integrated circuits (MMIC).

## 1 INTRODUCTION

Ferroelectric materials are popular due to their superior dielectric properties characterized by their high dielectric constant and polarization values. The review made by (Setter *et. al.*, 2006) discussed their dielectric properties and represented the state of the art development of the material - the domain structure and their effects on relative permittivity and loss, and their implication in micro-systems and high frequency device applications .

Lead zirconate titanate (PZT) and lead niobate zirconate titanate (PNZT) belong to the family of ferroelectric materials. Both are known for their high dielectric constant as well as their superior perovskite characteristics useful for high capacitor density applications (Dimos and Mueller, 1998, Riemens *et. al.* 2003 and Haccart *et. al.*, 2006). With

the addition of a dopant such as Nb, the PZT can demonstrate higher dielectric constant and promote larger perovskite crystals, as well as increased film resistivity (Souza *et.al.*, 2004). The addition of Nb also influences the film characteristics such as microstructure, as well as the electrical properties. Also, there is correlation between internal electric field and 'self polarization' of the films that increases with Nb concentration.

Souza *et.al.*, 2004 found that the enhancement of the piezoelectric and ferroelectric properties of PNZT is possible with careful control of the crystallographic orientation of the polycrystalline films or growing the epitaxial films with preferred orientation. Their study also investigated the film thickness effects on the ferroelectric and piezoelectric properties of PNZT thin films.

In our work, PZT and PNZT thin films prepared differently were utilized to explore their microwave

properties. The films were studied over two types of applications – as thin film metal-insulator-metal (MIM) capacitors, and as a new substrate material for the construction of co-planar waveguides. The principal motivation of this work was to exploit the high dielectric constant of these films to reduce the size of capacitors and transmission lines, two components which traditionally take up large area of MMIC. Thus using these ferroelectric films offer the potential of reducing the size of MMICs, leading to wireless systems having more efficient power consumption.

Two capacitor test structures of  $2500 \mu\text{m}^2$  area were fabricated on the films and measured by employing the planar circuit technique. The measurement was performed using *Cascade Microtech* wafer probes and a vector network analyzer with short-open-load (SOL) calibration technique. The measurements were carried out over a wide frequency range of 40 MHz to 20 GHz which are suitable for MMIC applications. The capacitance, loss tangent and relative permittivity of the films were then extracted from the experimental data. From the analysis, behavior of dielectric polarization of PNZT and PZT over a broad frequency range was deduced.

Various transmission lines were then constructed in co-planar form with both films acting as the substrate. The novelty of this work is to show the feasibility of using ferroelectric materials as the substrate for MMIC. This paper reports results of further investigations of our previous work, which has been extended to include tests on the various transmission line structures.

## 2 METHODOLOGY

The films were prepared using standard methods compatible with MMIC processing. The objectives of the experimental work made were to two-fold: to analyze the capacitance, loss tangent and their relative permittivity at microwave frequencies, and to measure the insertion loss of the films by analyzing the transmission lines constructed out of these films.

### 2.1 Sample Preparation

The PZT and PNZT samples were categorized based on the method of deposition, doping, dielectric thickness, orientation, crystallinity and grain size obtained from the X-ray diffraction (XRD). The PNZT films were grown using metal organic

deposition to give films of  $1 \mu\text{m}$  thick, while the PZT was prepared with RF sputtering with thicknesses of the order of  $0.5 \mu\text{m}$ . The PNZT films were tetragonal (20/80) and doped with 4 % Nb, while the PZT films were (50/50) cubic. The top metallization layers of the capacitor structures were Ti, while Pt was used as bottom electrodes.

### 2.2 Device Fabrication

The fabrication processes used are compatible with semiconductor processing, details of which are reported earlier (Bakar *et. al.*, 2008). The fabrication for PNZT sample was modified slightly due to the Pt etchant which attacked the PMMA photoresist used. For this sample, the capacitor test structures were delineated after the Pt layer was removed. Figure 1 shows the capacitor prototype with area  $50 \mu\text{m} \times 50 \mu\text{m}$ .

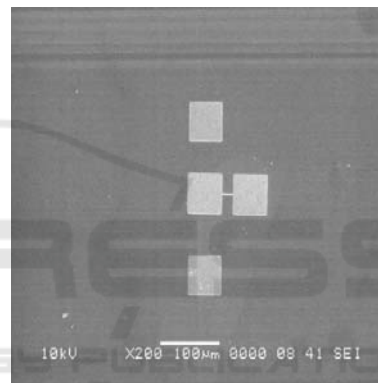


Figure 1: A typical thin film capacitor test structure constructed in this work, with ground-signal-ground (GSG) pads on the left for wafer probing.

### 2.3 Measurement

High frequency measurements were carried out on the capacitor using on-wafer probe and vector network analyzer (VNA). The SOL one-port calibration technique was performed for the capacitance measurements, while SOLT was employed to calibrate the two-port transmission line structures to minimize measurement errors due to parasitics (WinCal 3.2 User Guide, 2000). The Open standard in SOL was obtained by lifting the probe at least 0.25 mm in air, while the Short and  $50 \Omega$  standards were provided by the manufacturer impedance standard substrate (ISS). The probe tip placements were ensured to be consistent to achieve repeatable measurements and calibrations. The short standard defines a zero-length reference plane. The reflection coefficient,  $S_{11}$  of the test structure is obtained after the probe calibration is completed.

### 3 RESULTS AND DISCUSSION

#### 3.1 Capacitors

The S-parameter data obtained from the measurement consist of real and imaginary parts of the input impedance of the test structures. The complex permittivity of a dielectric is written as (Al-Omari and Lear, 2005);

$$\varepsilon^* = \varepsilon' - j\varepsilon'' \quad (1)$$

where the  $\varepsilon'$  is the real part that represents the relative dielectric constant which characterizes a material's ability to store charges. On the other hand,  $\varepsilon''$  is the imaginary part that describes the dielectric loss which is a measure of the dispersion in the material. The data is then used to extract the capacitance, relative permittivity and loss tangent of the films.

The impedance equation is shown in equation (2); where  $\varepsilon_0$  is the free space permittivity,  $A$  is the capacitor area which is  $2500\mu\text{m}^2$ ,  $d$  is the dielectric thickness and  $\omega$  is the angular frequency.

$$Z = \frac{d}{j\omega\varepsilon_0\varepsilon^*A} \quad (2)$$

The capacitance is calculated from  $S_{11}$  using :

$$\frac{d}{j\omega\varepsilon_0(\varepsilon' - j\varepsilon'')A} = Z_0 \left( \frac{1 + S_{11meas}}{1 - S_{11meas}} \right) \quad (3)$$

where  $S_{11meas}$  is the measured  $S_{11}$ . Using (3) the real and imaginary parts of  $\varepsilon' - j\varepsilon''$  give the following expressions (Park *et. al.*, 2002):

$$\varepsilon'(\omega) = \left( \frac{d}{\omega\varepsilon_0A} \right) \frac{1}{Z_0} \text{Im} \left( \frac{1 - S_{11meas}}{1 + S_{11meas}} \right) \quad (4)$$

$$\varepsilon''(\omega) = \left( \frac{d}{\omega\varepsilon_0A} \right) \frac{1}{Z_0} \text{Re} \left( \frac{1 - S_{11meas}}{1 + S_{11meas}} \right) \quad (5)$$

Both equations yield the frequency dependence of  $\varepsilon'$  and  $\varepsilon''$ . Subsequently, these equations are

made use to evaluate the capacitance, the relative permittivity as well as the loss tangent. The capacitance of the structure is obtained by relating the imaginary part of the impedance;

$$X_c = \frac{1}{j\omega C} \quad (6)$$

From the measured  $S_{11}$ , the impedance is calculated as in (4) using the equation:

$$Z = 50 \left( \frac{1 + S_{11meas}}{1 - S_{11meas}} \right) \quad (7)$$

The capacitance is extracted using the following equation:

$$C = \frac{1}{\omega \times 50 \times \text{Im} \left( \frac{1 + S_{11meas}}{1 - S_{11meas}} \right)} \quad (8)$$

The loss tangent is determined from the ratio of the imaginary and the real parts of (4) and (5) respectively;

$$\tan|\delta| = \frac{\varepsilon''}{\varepsilon'} \quad (9)$$

Details of our work have been reported elsewhere (Sulaiman *et. al.*, 2011), and hence only the main findings relevant to the discussion of our new results are repeated here. Figures 2 and 3 below show typical response of the dielectric properties over the frequency range mentioned. The PNZT films exhibited higher permittivity compared to PZT, this is expected due to the Nb doping. Both films showed decreasing trends of  $\varepsilon_r$  as the frequency is increased, again this is expected as the films get more lossy with frequency due to polarization.

As expected, the decrease in  $\varepsilon_r$  was accompanied by an increase in loss tan for both samples (Sulaiman *et. al.*, 2011). The values of  $\tan \delta$  for the PZT film were in the range of 0.04 to 0.18, while similar behavior were seen for PNZT. This response can be explained by the presence of the relaxation phenomena where as the frequency of electric field is increased, there is a point where the permanent electric dipoles of the material can no longer rotate fast enough to remain in phase with the field. Hence, these mechanisms reduce the polarization and

subsequently reduce the permittivity, while the loss tangent increases (Al-Omari and Lear, 2005).

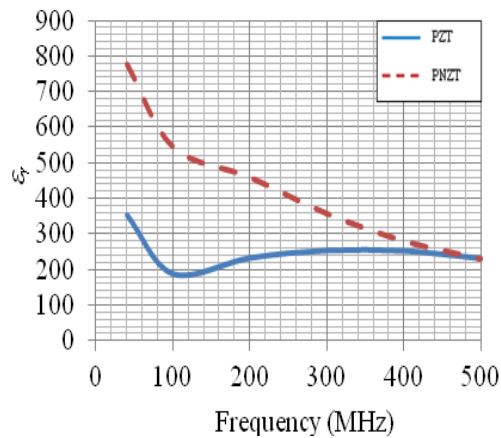


Figure 2: Permittivity versus frequency between 40 to 500 MHz.

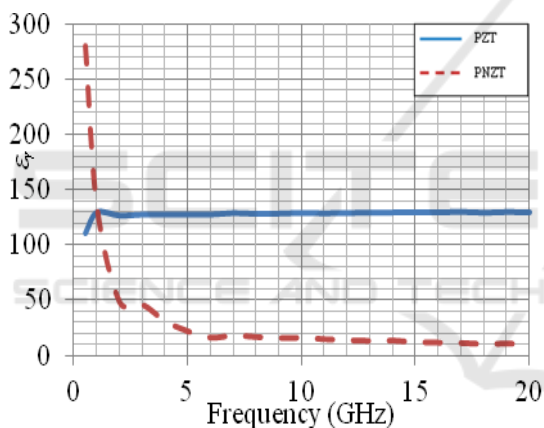


Figure 3: Permittivity versus frequency between 0.5 to 20 GHz

From the results we could see the effect of doping to PZT has significant impact on the capacitor performance.  $Nb^{5+}$  is a donor dopant which replaces the  $Zr^{4+}/Ti^{4+}$  ions in the B-site of PZT - this compensates the positive charge introduced (Riemens *et. al.*, 2003). Also, there is correlation between the grain size and  $\epsilon_r$  with Nb concentration. Riemens *et. al.*, 2003, Haccart *et. al.* 2003 and Souza *et.al.*, 2004 reported enhancement to  $\epsilon_r$  with Nb doping. However, the increase of  $\epsilon_r$  is also influenced by composition as well as Nb concentration. The work by Souza *et.al* 2004 showed that PNZT with high  $\epsilon_r$  has higher  $\tan \delta$  compared to PZT. Similar lossy behavior of PNZT in our samples is seen in Figures 2 and 3.

The drastic decrease of  $\epsilon_r$  with frequency for PNZT may be attributed to grain size as proposed by (Chikuvula, 2000). The degradation of  $\epsilon_r$  can be caused by several factors such as dielectric relaxation and microstructure defects (Dimos and Mueller, 1998; and Elisalde and Ravez, 2001). In addition, different types of polarizations (which are classified according to dipole type) can give rise to several dispersion regions over the broad frequency range. With the decreasing permittivity, therefore, the loss is expected to increase with frequency. This behavior was indeed observed for both our films over the two frequency ranges. Many factors contribute to dissipation in a ferroelectric material - among them is the effect of oxygen and lead vacancies (Park *et. al.*, 2002; Chang and Anderson, 1997 and Zhu *et. al.*, 2006), ferroelectric domain wall motion, as well as film composition and microstructure (Park, *et. al.*, 2002; and Elisalde and Ravez, 2001).

Table 1 summarizes the dielectric properties of our films from 40 MHz to 20 GHz, and compares with those of (Vilarinho, *et. al.*, 2005). Though the loss tangent in this work was higher, the permittivity values were in the expected range for both thin films.

Table 1: Comparison of material properties.

	$\epsilon_r$	$\tan \delta$
PZT (this work)	110 - 353	0.04 - 0.1
PNZT (this work)	11 - 778	0.15 - 1.18
Vilarinho <i>et. al.</i> 2005	200- 1000	0.01 - 0.07

### 3.2 Transmission Lines

To demonstrate the feasibility of using these films in MMIC, several transmission lines were constructed on them. The lines were designed in both microstrip and co-planar waveguide (CPW) form. The co-planar waveguide format is preferred for high frequency on-wafer probing due to the co-planar arrangement of the *Cascade* probes used in this work. The CPW is also preferred over microstrip in MMIC applications since the former eliminates the need to use via holes, which is difficult to realize, and model, in MMIC. An example of the co-planar waveguide line structure used in our work is shown in Figure 4.

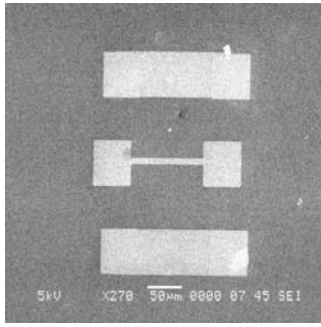


Figure 4: The test structure showing co-planar waveguide transmission line fabricated on PNZT film.

### 3.2.1 Simulation Results

#### a) Effect of $\epsilon_r$

The transmission lines were also simulated to predict their behavior. The *CST Microwave Studio* electromagnetic simulator was employed for this purpose. In the simulation,  $\epsilon_r$  values between 200 to 1000 were used to replicate the high- $k$  properties of the films. Figure 5 depicts the simulated insertion loss values of CPW lines for different  $\epsilon_r$ . The line length and width were set to 100  $\mu\text{m}$  and 5  $\mu\text{m}$  respectively. The CPW structure was treated as a symmetrical configuration, (Kuang *et. al.*, 2010; Pozar, 2005 and Kitzawa and Itoh, 1991) with the gap between the ground pad and the center conductor set to 50  $\mu\text{m}$  apart to comply with the GSG probe pitch limitation. The  $\tan \delta$  value was fixed to 1 as ceramic materials are normally lossy (Pozar, 2005; and Mirshekar-Syahkal, 1983). The results show that as  $\epsilon_r$  increases; the insertion loss increases with frequency. These results indicate that for a given frequency; as the relative permittivity is increased, the insertion loss is degraded. This is because more rf energy is lost in the dielectric as  $\epsilon_r$  is increased.

#### b) Effect of line geometry

The CPW was treated as symmetrical configuration throughout the simulation. The gap  $s$  was set to 50  $\mu\text{m}$  to comply with the probe pitch, while the centre strip line width  $w$  was varied. However, the minimum  $w$  is limited by the fabrication process. In this simulation the insertion loss was computed when  $w$  was varied over two sets of values - from 1 to 5  $\mu\text{m}$ , and from 5 to 50  $\mu\text{m}$ . The results of these two sets of simulations are shown in Figures 6 and 7 respectively.  $\epsilon_r$  for both

simulations were set at 200, and the line length was 100  $\mu\text{m}$  with loss tangent of 1. The electrode thickness was fixed at 0.26  $\mu\text{m}$ . The results in Figures 6 and 7 illustrate that  $S_{21}$  did not show a significant dependency on the line width. Both sets of results exhibit the same trend and comparable insertion loss values.

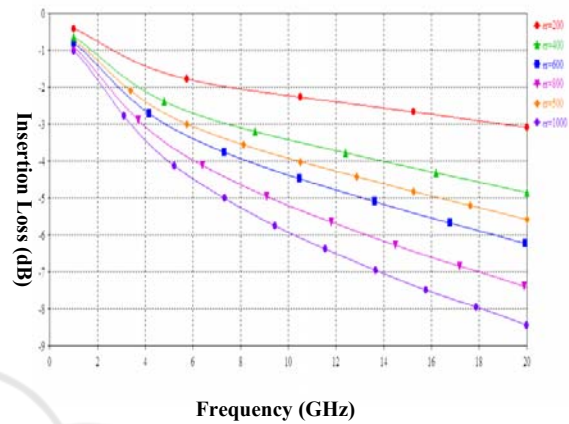


Figure 5: Variation of insertion loss of CPW lines with frequency for different  $\epsilon_r$  values: 200 (●), 400 (▲), 500 (◆), 600 (■), 800 (▼) and 1000 (◇).

Now, if the insertion losses are calculated with different

$$\frac{w}{w + 2s}$$

ratios at a fixed frequency of 10 GHz, the response obtained is shown in Figure 8 when  $w$  was varied from 5 to 50  $\mu\text{m}$ . It can be seen that the insertion loss remain almost unchanged when  $w$  was varied.

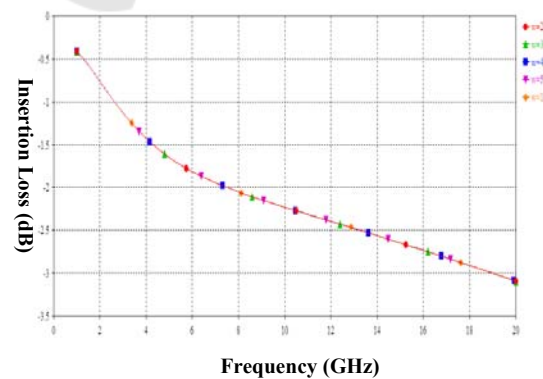


Figure 6: Variation of insertion loss with frequency for different line widths: 1  $\mu\text{m}$  (◆), 2  $\mu\text{m}$  (●), 3  $\mu\text{m}$  (▲), 4  $\mu\text{m}$  (■) and 5  $\mu\text{m}$  (▼).

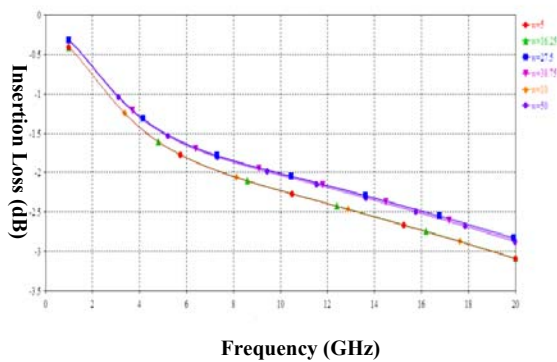


Figure 7: Variation of insertion loss with frequency for different line widths: 5  $\mu\text{m}$  ( $\bullet$ ), 10  $\mu\text{m}$  ( $\blacklozenge$ ), 16.25  $\mu\text{m}$  ( $\blacktriangle$ ), 27.5  $\mu\text{m}$  ( $\blacksquare$ ), 38.75  $\mu\text{m}$  ( $\blacktriangledown$ ) and 50  $\mu\text{m}$  ( $\bullet$ ).

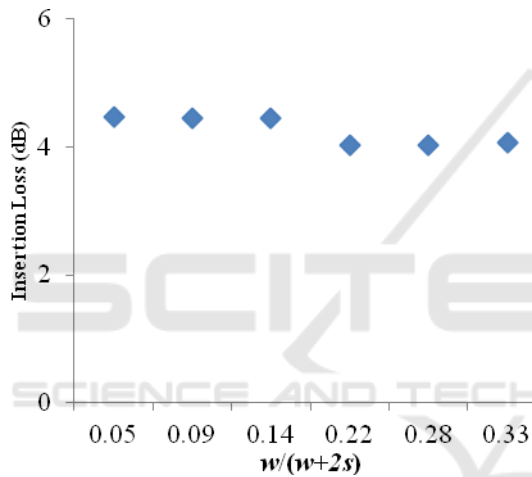


Figure 8: Insertion loss versus  $w/w+2s$  for  $w = 5$  to  $50 \mu\text{m}$  at 10 GHz.

Using the electromagnetic simulator the current density distribution over the conducting strip was examined. These are shown in Figures 9 and 10 for cases where the width is decreased gradually from 50  $\mu\text{m}$  to 16.25  $\mu\text{m}$ . It can be seen that when the width of the conducting strip is equal to those of the ground planes the currents are equally distributed (Figure 9), and as the width was reduced the current density in the center conductor decreased as well – this is expected since the line impedances are now higher.

Current crowding at the conductor edges may also affect the performance of a CPW besides conductor surface roughness (Wen, 1969 and Jackson, 1986). Using an electromagnetic simulator this current can be examined quite conveniently as shown in Figure 9. In this figure current crowding at

the conductor edge is revealed by plotting the current density across the width of the conductor. The current density values at the edge was about  $5.13 \times 10^7 \text{ A/m}^2$ , the arrows are more densely located at the conductor edges, indicating current crowding. As the metal thickness was set to be 0.26  $\mu\text{m}$ , which is less than the skin depth of Au at 10 GHz (0.8  $\mu\text{m}$ ); this implies that the rf current flow is concentrated at the edge of the lines in the slot region. In contrast, when the width-gap ratio decreases, as expected the current distribution in the center conductor decreases too (Riazat, 1990), as shown in the plot of current density in Figure 10.

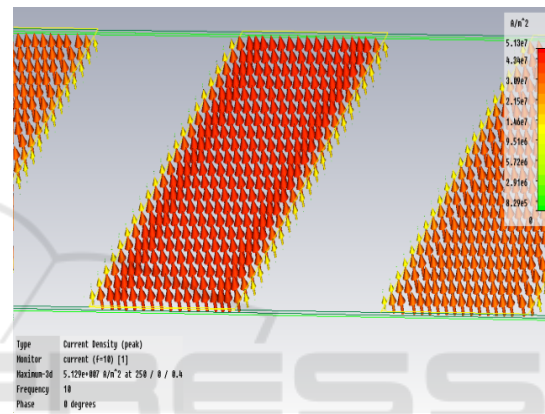


Figure 9: Current density of CPW for  $w = 50 \mu\text{m}$ .

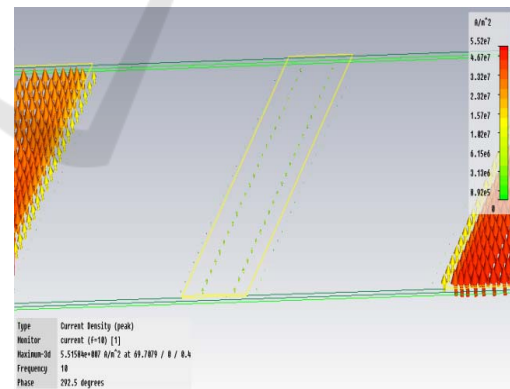


Figure 10: Current density of CPW for  $w = 16.25 \mu\text{m}$ .

### c) Effect of Film Thickness

As mentioned previously, the thicknesses of PZT and PNZT films were 0.5  $\mu\text{m}$  and 1.0  $\mu\text{m}$  respectively. In the simulation however, the film thicknesses were varied to investigate the CPW performance. The values of  $\epsilon_r$  and  $\tan \delta$  were obtained from the capacitance measurement: for

PZT they were 110 and 0.2, and for PNZT they were 280 and 1.

Figure 11 shows the result of this simulation for PNZT, where plots of  $|S_{21}|$  with PNZT film thicknesses varying from 1 to 5  $\mu\text{m}$ . Two things are clear from the figure: firstly we see that as the film gets thicker,  $|S_{21}|$  decreases, implying a reduction in the insertion loss. This behavior is expected because as the film gets thicker, its physical properties will be more uniform and approach those of bulk samples. This is supported by evidences reported in the literature (Zhi-Xiang *et al.*, 2008, Haccart *et al.*, 2003 and Riemens *et al.*, 2003) whereby bulk samples show better performance than thin films. Secondly,  $|S_{21}|$  also decreases with frequency, suggesting that the films get more lossy with frequency. This is due to the fact that at elevated frequencies the charges in the films are unable to switch to the higher frequency electric field. From the graphs it is important to note that for practical integration circuit applications, it is advisable not to use films thinner than 1  $\mu\text{m}$  since the losses degraded quickly after that. In this work, the films used were 1  $\mu\text{m}$  thick since it is quite difficult to get thicker films using metal organic deposition.

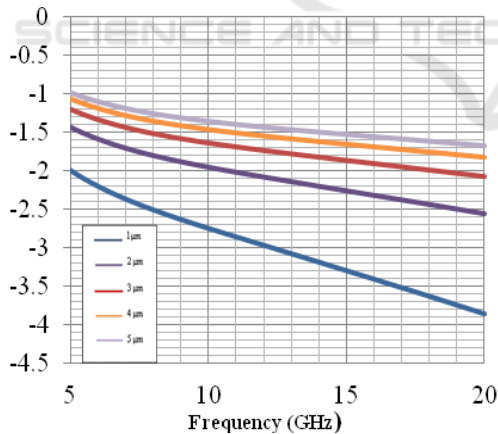


Figure 11:  $|S_{21}|$  versus frequency for PNZT films of varying thicknesses.

### 3.2.2 Measurement Results

Test structures in the form of planar circuits such as stripline, microstrip and co-planar waveguide are commonly used for material property characterization at microwave frequencies. These

test structures consist of dielectric substrates and conductors that act as conducting strips and grounding conductors. Microwave measurements are made to examine the effect of substrate property and conductor geometry so that microwave properties of the circuit can be analyzed (Chen *et al.* 2004).

In this work, experimental investigations of the microwave behavior of both PZT and PNZT thin films were performed using microstrip and co-planar waveguide structures. In each structure, the PZT and PNZT films which acted as a dielectric supported by the silicon substrates.

The fabrication of the co-planar waveguide and microstrip transmission lines was identical for both films. The width and length of the lines are 5  $\mu\text{m}$  and 100  $\mu\text{m}$  respectively. The structures were measured with wafer probes in conjunction with a vector network analyzer for high frequency characterization. Measurement calibrations were performed using the SOLT technique, aided by the ISS impedance standard supplied by the probe manufacturer. Two-port measurements were carried out to evaluate the insertion loss of the films over a frequency range of 5 GHz to 20 GHz.

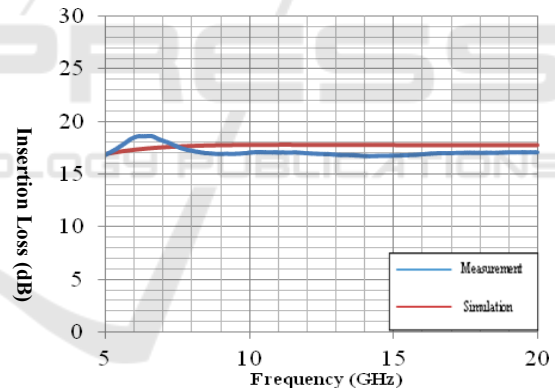


Figure 12: Comparison of simulated and measured insertion loss values of PNZT-based CPW.

Figure 12 shows the plot of one such result for PNZT-based CPW, shown together with the computer simulation for comparison. Both traces show the same trend, and the agreement is quite good, although the simulated values were slightly higher. The results are the evidence that PNZT can be used as a dielectric material in a CPW. The slight discrepancies between the two results were probably due to the mismatch loss that occurred in PNZT films and to factors other than substrate properties – this may include errors in the calibration and device fabrication, and the electrode behaviour at high

frequency. The mismatch happened due to the fact the transmission lines were not exactly  $50 \Omega$  – with the high dielectric constants exhibited by the films, the line width required to give  $50 \Omega$  was too small to be realized with our fabrication facilities. The difference in the impedance of the line and that of the probes would have given rise to reflections at the input port, and this resulted in mismatch loss. In addition, the loss of the PNZT-based CPW might not only be due to the properties of the thin films themselves, but to the geometrical aspects of the transmission lines as well.

In the course of our work we found better agreements with simulation were observed for PNZT samples. We also found the PZT samples exhibited higher insertion losses compared to PNZT of the same line dimensions and film thickness. PNZT-based CPW as a whole generally showed better all round performance in our work.

In order to determine the film properties, as well as to investigate the effect of microwave frequency on PNZT as a high- $k$  material; a parametric study was carried out by varying the film parameters, to fit the simulation results with measurements. The line dimensions were actual ones used in the fabrication, while the film parameters such as  $\epsilon_r$  and  $\tan \delta$  were varied. The effects of these variations on the insertion loss are shown in Figures 13 and 14 respectively.

Figure 13 a) shows that as the loss tangent is increased, the fit is better. This is expected from theory since in a transmission line, the insertion loss is mainly due to energy dissipation in the substrate (in this case the ceramic film) – a material with high loss tangent implies significant energy loss in the material, and this leads to high insertion loss. Ceramic materials in thin film form are known to be quite lossy, and our results seem to concur with this. In this example, a good fit between measurement and simulation is obtained for  $\epsilon_r = 200$  and  $\tan \delta = 1$  as shown in Figures 13 a) and b) respectively. Nevertheless our work has demonstrated that it is possible to implement PNZT and PZT thin films for use in MMIC.

## 4 CONCLUSIONS

PZT-based and PNZT-based thin film capacitors have been fabricated and their performance compared to investigate the effect of polarization at high frequencies. The high frequency measurement is divided into two frequency ranges; 40 MHz to 500 MHz and 500 MHz to 20 GHz. The results

reveal that Nb doping affect the relative permittivity of the films, but the losses increased at high frequencies. The relative permittivity values were higher for PNZT films as expected due to doping.

The insertion loss characteristics of the films were studied by implementing co-planar waveguide transmission lines on PNZT. The films showed acceptable performance and proved the feasibility of using the films as a new substrate material for microwave integrated circuits. Our future work will include the use of these materials in the design of passive MMIC devices such as filters and phase shifters.

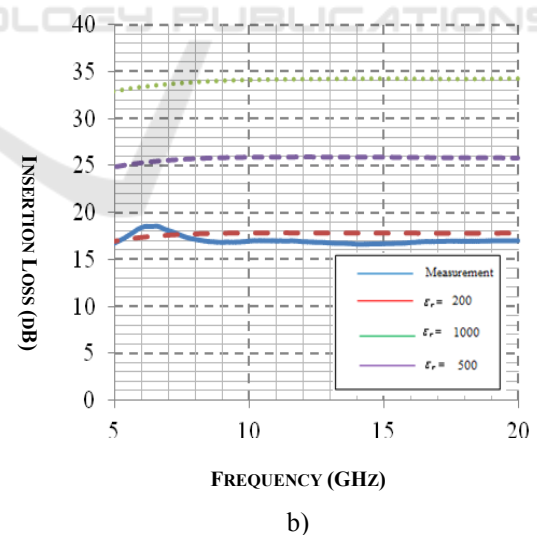
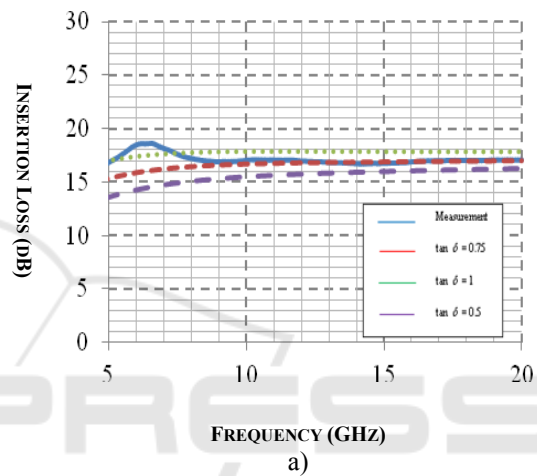


Figure 13: Comparison between simulated and measured results of PNZT-based CPW transmission lines; with adjusted a)  $\tan \delta$  and b)  $\epsilon_r$ .

## ACKNOWLEDGEMENTS

The authors would like to thank Prof. Dr. Mohamad Rusop and his team from the Nanotechnology Research Group of University Technology MARA for the assistance given in the fabrication. We are also grateful to Dr. Sukreen Hana Herman for the PZT thin film samples used in this work.

## REFERENCES

- Al-Omari A. N. and Lear K. L. 2005. *Dielectric Characteristics of Spin-Coated Dielectric Films using On-wafer Parallel-Plate Capacitors at Microwave Frequencies*. IEEE Trans. on Electrical Insulation, 12, 1151-1161.
- Bakar R. A. et. al. 2008. *Optimized Fabrication Process of PZT Thin Film Capacitor for MMIC Applications*, Proc. Int. Conf. on Nanosc. and Nanotech., Shah Alam, Malaysia, Nov 18 – 21.
- Chang L. H. and Anderson W. A. 1997. *Single and Multilayer Ferroelectric PZT on BaTiO<sub>3</sub>*. Thin Solid Films, 303, 94-100.
- Chen L. F. et. al. 2004. *Microwave Electronics: Measurement and Material Characterization*. New York: John Wiley & Sons, Ltd., 382.
- Chikuvula, V. et. al. 2000. *Ferroelectric Dielectric for Integrated Circuit Applications at Microwave Frequencies*, US Patent 6146905.
- Dimos D. and Mueller C. H., 1998. *Perovskite Thin Films for High-Frequency Capacitor Applications I*, Annual Reviews in Materials Science, 28, 397-419.
- Elissalde C. and Ravez J. 2001. *Ferroelectric Ceramics: Defects and Dielectric Relaxations*, J. of Mat. Chem., 11, 1957-1967.
- Haccart T. et. al. 2003. *Substitution of Nb Doping on the Structural, Microstructural and Electrical Properties in PZT Films*, Thin Solid Films, 423, 235-242.
- Jackson R. W. 1986. *Considerations in the Use of Coplanar Waveguide for Millimeter-Wave Integrated Circuits*, IEEE Trans. on Microwave Theory and Tech., 34 (12), pp. 1450-1456.
- Kitzawa T. and Itoh T. 1991, *Propagation Characteristics of Coplanar Type Transmission Line with Lossy Media*, IEEE Trans. on Microwave Theory and Technique , 39 (10), 1694-1700.
- Kuang, K. et. al. (eds). 2010. *RF and Microwave Microelectronics Packaging*. Netherlands: Springer Science + Business Media.
- Mirshekar-Syahkal, D. 1983, *An Accurate Determination of Dielectric Loss Effect in Monolithic Microwave Integrated Circuits Including Microstrip and Coupled Microstrip Lines*, IEEE Trans. on Microwave Theory and Tech., 31(11), 950-953.
- Park Y. et. al. 2002. *Effect of Excess Pb on Fatigue Properties of PZT Thin Films Prepared by Rf-Magnetron Sputtering*. Mat. Lett., 56, 481-285.
- Pozar, D. M. 2005, *Microwave Engineering*, 3rd ed. New York: John Wiley & Sons Inc.
- Riaziat M. et. al., 1990. *Propagation Modes and Dispersion Characteristics of Coplanar Waveguide*, IEEE Trans. on Microwave Theory and Tech., 38 (3), pp. 245-251.
- Riemens D. et. al, 2003. *Piezoelectric Properties of Sputtered PZT Films: Influence of Structure, Microstructure, Film Thickness (Zr,Ti) Ratio and Nb Substitution*, Materials Science in Semiconductor Processing, 5, 123-127.
- Setter N. et. al., 2006. *Ferroelectric Thin Films: Review of Materials, Properties and Applications*, J. App. Phys, 100, 510-606.
- Souza, E. C. F. et.al. 2004. *The Effect of Nb Doping on Ferroelectric properties of PZT Thin Films Prepared from Polymeric Precursors*, Materials Chemistry and Physics, 88, 155-159.
- Sulaiman, S., Nadzar H. M. and Awang, Z. 2011, *Characterization of PZT and PNZT thin films for monolithic microwave integrated circuit applications*, Proc. 2011 IEEE Region 10 Conf. (TENCON2011), pg. 1264 – 1268, Nov. 22 – 24, Bali, Indonesia.
- Vilarinho, P. M. et al. (eds.). 2005. *Scanning Probe Microscopy: Characterization, Nanofabrication, and Device Application of Functional Materials*. Netherlands: Kluwer Academic Publishers, 3-33.
- Wen C. P. 1969. *Coplanar Waveguide: A Surface Strip Transmission Line Suitable for Non-reciprocal Gyromagnetic Device Applications*. IEEE Trans. on Microwave Theory and Tech., 77 (12), pp. 1087-1090.
- WinCal 3.2 User Guide. 2000, Cascade Microtech, Inc.
- Zhi-Xiang et. al. 2008. *Thickness and Nb-Doping Effects on Ferro and Piezoelectric Properties Highly a-axis Oriented Nb-doped Pb(Zr<sub>0.3</sub>Ti<sub>0.7</sub>)O<sub>3</sub> Films*. J.of App. Phys., 140, pp. 2003-2007, 2008.
- Zhu C. et. al. 2006. *The Effects of the PbO Content and Seeding Layers upon the Microstructure and Orientation of Sol-gel Derived PZT Films*. J. Mat. Sc.: Materials in Electronics, 17, 51-55.